11-2019

Synthesis and Application of Ce-doped TiO_2 Nanoparticles Loaded on Activated Carbon for Ultrasound-assisted Adsorption of Basic Red 46 Dye

Ebrahim Alipanahpour Dil
Yasouj University

Mehrorang Ghaedi
Yasouj University

Arash Asfaram
Yasouj University

Fatemah Mehrabi
Islamic Azad University, Iran

Ali Akbar Bazrafshan
Yasouj University

See next page for additional authors

Ultrasonics Sonochemistry, Vol. 58 (November 2019): 104702. DOI.

Synthesis and Application of Ce-doped TiO_2 Nanoparticles Loaded on Activated Carbon for Ultrasound-assisted Adsorption of Basic Red 46 Dye

Ebrahim Alipanahpour Dil
Department of Chemistry, Yasouj University, Yasouj 75918-74831, Iran
Mehrorang Ghaedi
Department of Chemistry, Yasouj University, Yasouj 75918-74831, Iran
Arash Asfaram
Medicinal Plants Research Center, Yasuj University of Medical Sciences, Yasuj, Iran
Fatemeh Mehrabi
Young Researchers and Elite Club, Gachsaran Branch, Islamic Azad University, Gachsaran, Iran
Ali Akbar Bazrafshan
Department of Chemistry, Yasouj University, Yasouj 75918-74831, Iran
Lobat Tayebi
Marquette University School of Dentistry, Milwaukee, WI

Abstract

Ce was doped on TiO_2 nanoparticles (NPs), and this association was loaded on activated carbon (Ce-TiO_2-NPs-AC). The characterization was completed by FE-SEM, TEM, and XRD, and finally these NPs were used for the ultrasonic-assisted adsorption of Basic Red 46 (BR 46) from aqueous solution. An experimental model suggested by the central composite design (CCD)—as a branch of response surface methodology (RSM)—provides insight into the influence of variables, such as BR 46 concentration, pH, adsorbent mass, and sonication time, on BR 46 removal. Experimental results revealed that setting conditions at 25 mg L^{-1} of BR 46, pH 5.0, 0.02 g of Ce-TiO_2-NPs-AC and 4 min sonication resulted in a high coefficient of determination ($R^2 > 0.99$) and low probability values. The difference in the values is likely due to the accumulation of more than 99% of BR 46, while equilibrium data described by Langmuir isotherm model with a high adsorption capacity of 58.61 mg g^{-1} and adsorption process were successfully correlated with pseudo-second-order kinetics model.

Graphical abstract

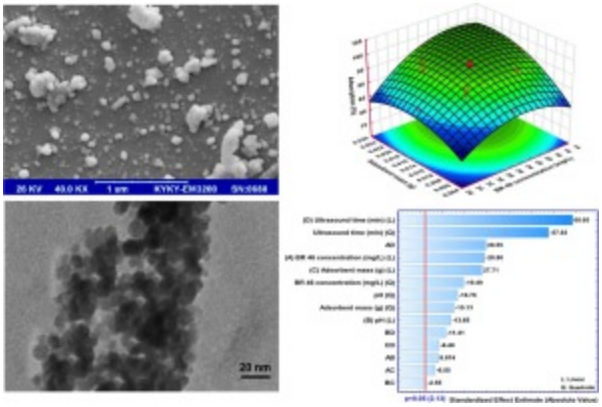

Keywords

Ce-TiO_2-NPs-AC, Ultrasound-assisted adsorption, Basic Red 46 dye, Central composite design

1. Introduction

Dyes—due to their extensive application in various activities—have a prominent role in industries such as textile, paint, and pigment manufacturing. However, dye waste can lead to the pollution of water and consequently induces skin irritation, respiratory problems, and cancer risk in humans and other living things. Accordingly, the removal of such waste from these media is highly recommended for maintaining high quality water resources [1], [2], [3].

Peer-reviewed literature reveals the ability of precipitation, coagulation, reverse osmosis, ozonation, and adsorption to achieve this requirement. Using these processes restricts their application, mainly due to their economic limitations and less effective generation of a large quantity of secondary sludge [4], [5], [6]; however, these drawbacks can be resolved. Adsorption methods provide benefits such as cost effectiveness, simplicity, and superiority in terms of operation and large capacity [7], [8], [9] and through using nanomaterials. It has extensively been denoted that the

performance of nanomaterials could significantly be improved via its high surface areas and the number of reactive unsaturated centers, which their combination with activated carbon (AC) results in the appearance of functional centers like OH, COOH, and NH and their cooperation with metallic nano-centers strongly improves capacity and reduces process time. Additionally, reduction in the internal diffusion resistance and the large specific area and also the presence of porous structure assigned to nanoparticle (NP) sorbents causes higher efficiency, using a small amount over a short time period [10], [11], [12], [13], [14].

Combination of nanostructure-based adsorption with ultrasound assists in decolorization stage by enhancing mass-transfer efficiency, which is likely the result of secondary effects such as cavitation, defied as nucleation, growth, and transient collapse of tiny gas bubbles. This phenomenon induces microstreaming, micro-turbulence, acoustic or shock waves, and micro-jets without significantly changing the equilibrium features of the adsorption/desorption system. Sonication is an effectual tool for strengthen the mass process between adsorbate and adsorbent [15], [16].

Parameter optimization is generally achieved by the statistical design of experiment (DOE) methods, and response surface methodology (RSM) enables multivariable optimization [17], [18], [19], [20], [21]. In this study, Ce-TiO_2-NPs-AC was synthesized and characterized using XRD, FE-SEM, and TEM and utilized for the ultrasound-assisted adsorption of Basic Red 46 (BR 46). Correlation among four response variables—pH, initial BR 46 concentration, adsorbent mass, and ultrasound time was investigated by using central composite design (CCD).

2. Experimental

2.1. Instruments and reagents

All chemicals such as titanium isopropoxide, cerium nitrate, Basic Red 46 (BR 46, AC, NaOH, and HCl—were acquired from Merck, Darmstadt, Germany. Each solution in double distilled water was diluted, and the subsequent stages were accomplished according to our previous publications [11], [13], [22].

2.2. Ultrasound-assisted synthesis of Ce-TiO_2-NPs-AC

Typical synthesis procedure based on ultrasound was as follows: a mixture of 50 mL of 2-propanol and 5 mL of titanium isopropoxide was taken in a 250-ml beaker, which was then put in a constant temperature bath. Sonication process was conducted by using a direct immersion titanium horn in the sonication cell, in order to retain the ratio (2% mole) of Ce to TiO_2 in distilled water (20 mL). Subsequently, sodium hydroxide (5 mL) and cerium nitrate (2 mL) solutions were added at the same time every 30 s until the achievement a final volume of 70. This resultant solution transferred to an ultrasound reactor and sonicated for additional 30 min. After irradiation for 30 min, the solution was kept constant to settle the precipitate, which was later centrifuged, filtered, dried, and calcined at the temperature of 450 °C for a time period of 3 h [23]. Finally, the prepared Ce-TiO_2-NPs mixture was agitated with AC (1:10), set in a thermo-bath at the temperature of 80 °C for 8 h and left at room temperature to be dried.

2.3. Ultrasound-assisted adsorption procedure

Ultrasound-assisted adsorption experiments were employed to investigate the influence of different parameters on Ce-TiO_2-NPs-AC for the adsorption of BR 46; the procedure has been described in detail in our previous publications [21], [24].

2.4. Rsm

In the field of water and waste water treatment, RSM was used for the optimization of process, which its detailed description is available in our previous publications [25], [26].

3. Results and discussion

3.1. Characterization of Ce-TiO_2-NPs

FE-SEM results of surface morphology of Ce-TiO_2-NPs, as represented in Fig. 1(a), indicated that particles had uniform distribution, spherical morphology, and slight agglomeration. The peaks and relative intensities in Fig. 1(b) reveal that Ce-TiO_2-NPs are matched to the standard pattern (JCPDS card no. 21-1272). Besides, the 2-theta at 25.28°, 36.88°, 37.80°, 38.51°, 48.05°, 53.76°, and 54.5° correspond to the crystal forms of (1 0 1), (1 0 3), (0 0 4), (1 1 2), (2 0 0), (1 0 5), and (2 1 1) of the anatase, respectively. Fig. 1(c) showing the TEM image of Ce-TiO_2-NPs displays their aggregation with porous nature. The TEM measurement of NPs size is ~20 nm, which agrees well with the Debye-Scherer calculation from FWHM of the (1 0 1) peak.

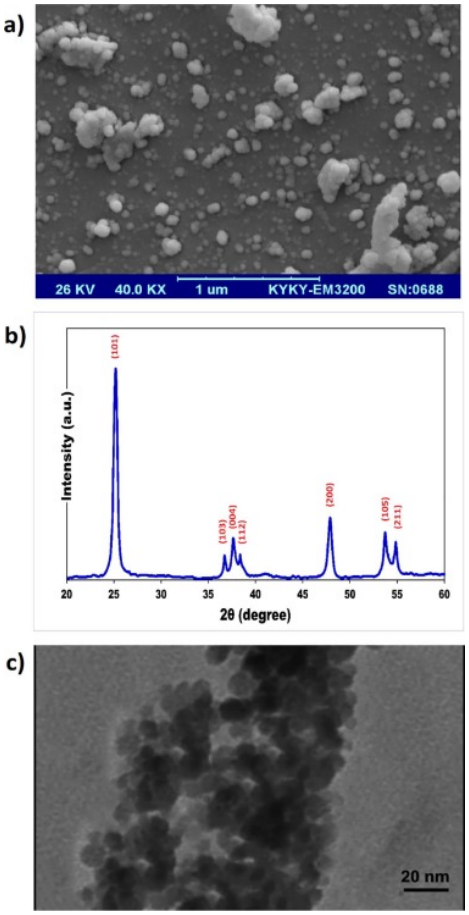

Fig. 1. FE-SEM (a), XRD (b), and TEM (c) of Ce-TiO_2-NPs.

3.2. Modeling the process and statistical analysis

Optimum conditions for BR 46 adsorption onto Ce-TiO_2-NPs-AC were determined through conducting experiments with the following parameters: BR 46 concentration (A: 15–35 mg L^{-1}), pH (B: 2–10), adsorbent mass (C: 5–25 mg), and sonication time (D: 1–5 min) (Table 1). To estimate the importance of each parameter, it is required to determine the significance of the quadratic model developed by the analysis of variance (ANOVA) from F-test and p-value. The large F-value, which is explained by the developed regression equation, suggests most variations in the output. The p-value was employed to evaluate whether F is large enough to show the statistical significance. As a result, if p-value is lower than 0.05, it denotes that the developed model and variables are statistically significant of [27]. The significance and adequacy of the regression model and the results were justified by ANOVA (Table 2). The F- and p-values in this Table display that the individual, second-order, and all the interaction variables are significant. The p-value of the reduced quadratic model was less than 0.0001, corroborating the excellent adjustment of the experimental data.

Table 1. Design matrix for the CCD.

Factors	**Levels**				
	−α	**Low (−1)**	**Central (0)**	**High (+1)**	**+α**
A: BR 46 concentration (mg L^{-1})	15	20	25	30	35
B: pH	2	4	6	8	10
C: Adsorbent mass (g)	0.005	0.01	0.015	0.020	0.025
D: Ultrasound time (min)	1	2	3	4	5

Run	**A**	**B**	**C**	**D**	**Adsorption (%)**
1	25	6	0.015	3	97.475
2	30	4	0.010	4	96.210
3	20	4	0.010	2	86.914
4	25	6	0.015	3	97.424
5	25	6	0.015	5	91.644
6	20	8	0.010	4	90.216
7	25	6	0.005	3	89.062
8	25	10	0.015	3	90.540
9	30	8	0.020	2	82.958
10	20	4	0.020	4	99.479
11	30	6	0.020	2	83.433
12	25	6	0.015	1	71.741
13	15	6	0.015	3	96.078
14	25	6	0.015	3	97.201
15	20	8	0.010	2	86.389
16	30	4	0.020	4	97.822
17	20	4	0.010	4	95.784
18	20	8	0.020	2	92.271
19	30	8	0.010	4	94.033
20	25	6	0.015	3	97.707

21	20	4	0.020	2	94.326
22	35	6	0.015	3	88.323
23	25	6	0.015	3	98.011
24	25	6	0.025	3	97.728
25	30	4	0.010	2	76.762
26	30	8	0.020	4	94.883
27	30	8	0.010	2	79.283
28	25	2	0.015	3	95.318
29	25	6	0.015	3	97.961
30	20	8	0.020	4	93.810

Table 2. Analysis of variance (ANOVA) for adsorption of BR 46.

Source	**Sums of squares**	**Df**[a]	**Mean squares**	**F-value**	**p-value**
Model	1433.9	14	102.42	798.50	<0.0001
A	106.79	1	106.79	832.58	<0.0001
B	23.911	1	23.911	186.41	<0.0001
C	98.488	1	98.488	767.83	<0.0001
D	604.59	1	604.59	4713.5	<0.0001
AB	8.3595	1	8.3595	65.172	<0.0001
AC	5.4975	1	5.4975	42.860	<0.0001
AD	112.00	1	112.00	873.18	<0.0001
BC	0.83375	1	0.83375	6.5001	0.02222
BD	16.706	1	16.706	130.24	<0.0001
CD	9.0437	1	9.0437	70.506	<0.0001
A^2	48.735	1	48.735	379.94	<0.0001
B^2	36.020	1	36.020	280.82	<0.0001
C^2	29.377	1	29.377	229.03	<0.0001
D^2	428.99	1	428.99	3344.5	< 0.0001
Residual	1.9240	15	0.12827		
Lack of Fit	1.4131	10	0.14131	1.3829	0.37869
Pure Error	0.51092	5	0.10218		
Corr. Total	1435.8	29			

Model Summary Statistics			
Standard deviation (SD)	0.35815	R-square	0.99866
Mean	91.693	Adj R-square	0.99741
Coefficient of variation (CV%)	0.39059	Pred R-square	0.99377
PRESS[b]	8.9393	Adequate precision	110.56

[a]Degrees of freedom.

[b]Predicted residual error sum of squares.

The correlation coefficients (R-square, adjusted (Adj) and predicted (Pred) R-square) are a good indication of model accuracy. Accordingly, an R-square value of 0.9998 for the quadratic model confirms the excellent ability of the model to fit the experimental data, which fully agrees with the Adj R-square value of 0.9991. The value of Pred R-square for the current model was 0.8547 (Fig. 2(a)), which shows acceptable agreement between predicted versus actual data. The adequate precision value was observed to be 114.75 (signal to noise ratio). This value is much greater than the critical value of 4, which obviously shows a strongly adequate signal it. The lack of fit (0.345) was not significant, and this insignificant result is favorable for the fitness of the data in the model. Regression analysis was utilize for the development of the best-fit model by using the collected data and empirical polynomial quadratic model, which is applicable to the predication of BR 46 adsorption as follows:

(1)

$$\begin{aligned}\mathrm{BR46adsorption} = \; & 25.34 + 0.54\mathrm{A} + 3.0\mathrm{B} + 2847.7\mathrm{C} + 21.0\mathrm{D} + 0.08\mathrm{AB} - 23.73\mathrm{AC} + 0.54\mathrm{AD} - 24.20\mathrm{BC} \\ & - \; 0.54\mathrm{BD} - 152.16\mathrm{CD} - 0.053\mathrm{A}^2 - 0.29\mathrm{B}^2 - 41479\mathrm{C}^2 - 3.96\mathrm{D}^2\end{aligned}$$

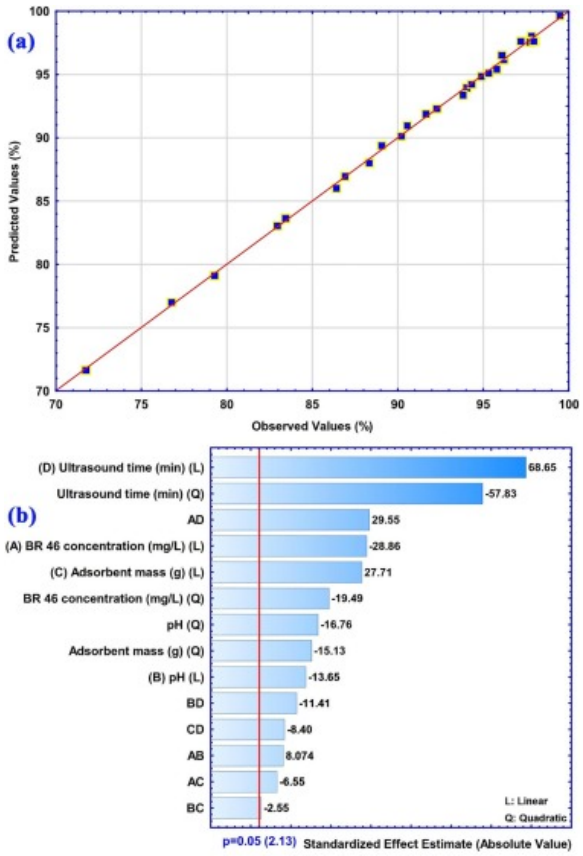

Fig. 2. Correlation of experimental and predicted values (a) and Pareto chart (p = 0.05) of CCD, which represents the estimated effects of parameters and interactions on adsorption of BR 46 (b).

Fig. 2(b) shows the analysis of the results by using standardized main effect Pareto chart (P = 95%) and also displays the quadratic and interaction effects of the variables. The analysis of results by Pareto chart was also confirmed by mathematical equation, which showed that the ultrasound time has the largest influence on the adsorption of BR 46. These observations support that sonication after the lateral formation of cavitation causes a high contact area and higher concentration gradient. Hence,

enhancement in the diffusion coefficient, as well as in the rate and magnitude of mass transfer via diffusion leads to the improvement of the migration.

3.3. Three-dimensional (3D) response surface plots

The 3D response surfaces plots, as the functions of two variables at the center level of other variables, are demonstrated in Fig. 3 and reflect the presence of interactions among variables. As seen in Fig. 3a, BR 46 adsorption is strongly dependent on adsorbent mass, while the opposite trend was found in its concentration (lower adsorption percentage at higher BR 46 value). The BR 46 residual concentration sharply increased at higher pH, which is due to pH changes from 2.0 to 10.0. The lower pH (between 2.0 and 5.0; Fig. 3b) is proportional with lower adsorption efficiency in comparison to higher pH. At lower pH values, the H^+ ions compete with the cationic form of BR 46, which reduces the adsorption efficiency. Despite the negative charge of the adsorbent due to the compromise of different forces like hydrogen bonds and π-π bonding in addition to electrostatic interaction, higher pH values led to the improvement in removal percentage [28]. Maximum dye adsorption achieved at 4.0 min sonication directly denotes quick equilibrium (Fig. 3b), which is likely related to the improvement in mixing, porosity, and diffusion coefficient.

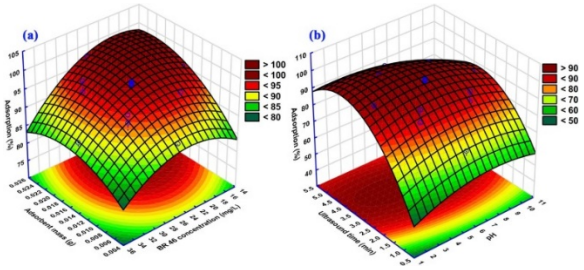

Fig. 3. The 3D response surfaces plot for the ultrasound-assisted adsorption of BR 46 dye.

3.4. Optimization of CCD by desirability function for BR 46 adsorption

Maximum BR 46 removal (99.86%) by Ce-TiO_2-NPs-AC occurs when experimental conditions (Fig. 4) are set at 25 mg L^{-1} of BR 46, pH 5.0, 0.02 g of Ce-TiO_2-NPs-AC in the presence of 4 min sonication. Suitability of these conditions was checked experimentally through the replication of five similar runs, which have an efficiency of 99.31% ± 1.64 of BR 46, and according to *t*-test, they do not statistically differ from each other.

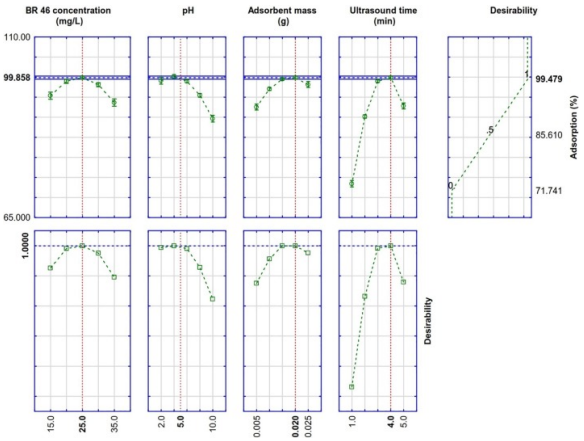

Fig. 4. Optimization plot for the adsorption of BR 46 by Ce-TiO_2-NPs-AC.

3.5. Adsorption kinetics

An ideal pollution control and removal must simultaneously be large capacity, based on adsorbent that is able to remove large content of pollutants in a short time. Therefore, the adsorption rate has a significant contribution on selection of adsorbent, and adsorption kinetics must be taken into account due to its ability to explain how fast the chemical reaction occurs and provide information on the factors affecting the reaction rate [29]. Kinetic modeling simultaneously represents adsorption rates and enables the evaluation of suitable rate expressions, while also guiding and justifying efficient reaction mechanisms [30]. In this respect, conventional previous models are applied to evaluate experimental data at 25 mg L^{-1} of BR 46. Pseudo first-order model is represented as [31]:

(2)

$$\log(q_e - q_t) = \log q_e - \left(\frac{k_1}{2.303}\right)t$$

Pseudo second-order model is represented as [32]:

(3)

$$\frac{t}{q_t} = \frac{1}{k_2 q_e^2} + \frac{t}{q_e}$$

The Elovich model is represented by [33]:

(4)

$$q_t = \frac{1}{\beta}\ln(\alpha\beta) + \frac{1}{\beta}\ln t$$

and, finally, intra-particle diffusion model is represented by [34]:

(5)

$$q_t = K_{diff} t^{1/2} + C$$

The results corresponding to the above model (Table 3) is depicted. Respective constants corresponding to each model is calculated and judgment determines that the pseudo second-order kinetic model best fits the BR 46 adsorption.

Table 3. Kinetic parameters for adsorption of BR 46.

Model	**Parameters**	**Value**
Pseudo-first-order kinetic	k_1 (min^{-1})	2.18
	$q_{e\ (calc)}$ (mg g^{-1})	7.04
	R^2	0.826
Pseudo-second-order kinetic	k_2 (min^{-1})	5.83
	$q_{e\ (calc)}$ (mg g^{-1})	53.91

	R^2	0.999
Intraparticle diffusion	K_{diff} (mg g^{-1} $min^{-1/2}$)	6.52
	C (mg g^{-1})	24.52
	R^2	0.986
Elovich	β (g mg^{-1})	0.638
	α (mg g^{-1} min^{-1})	1857.42
	R^2	0.851
Experimental data	$q_{e\ (exp)}$ (mg g^{-1})	48.63

3.6. Adsorption isotherms

Adsorption isotherms, which represent interaction among species, are the best choice to assess mechanism of process [29], and Langmuir isotherm as monolayer adsorption has the following relationship [35]:

(6)

$$\frac{C_e}{q_e} = \frac{1}{Q_m k_L} + \frac{C_e}{Q_m}$$

This equation well defines the slope and intercept of line corresponding to drawing C_e/q_e vs. C_e, which is applied for estimation of Q_m and K_L.

The Freundlich equilibrium adsorption curves has unique properties. Based on parameters like 1/n, K_F and q_e [36], each research can understand mechanism and ability of model for good representation of experimental data.

(7)

$$\log q_e = \log K_F + \frac{1}{n}\log C_e$$

This isotherm dose does not predict any saturation of nitrogenous adsorbent surface. The Freundlich constants viz. K_F and 1/n can be determined from intercept & slope of the linear plot of log q_e vs. log C_e. To evaluate heat of adsorption and coverage magnitude over adsorbent, the adsorption data is analyzed through following linear equation (eq. (8)) [37], [38]:

(8)

$$q_e = B_1 \ln k_2 + B_1 \ln C_e$$

The most useful model from Dubinin–Radushkevich [39] is given as:

(9)

$$\ln q_e = \ln Q_s - K\varepsilon^2 \frac{1}{n}$$

where ε can be correlated:

(10)

$$\varepsilon = \mathrm{RT}ln\left(1 + \frac{1}{\mathrm{C_e}}\right)$$

The isotherm parameters obtained from fitting the curves to the Langmuir, Freundlich, Temkin and Dubinin-radushkevich models are given in Table 4. However, according to judgment based on correlation coefficients (R^2), the Langmuir model is superior to the others models to describe understudy system. The results suggest that the adsorbent is homogeneous and the adsorption film has monolayer coverage, since its reasonable maximum monolayer adsorption capacity is recommended for further study. The adsorption capacities of Ce-TiO_2-NPs-AC obtained from Langmuir isotherm model is found to be moderately higher than that of many adsorbents reported in the literature (Table 5).

Table 4. Isotherm constant parameters and correlation coefficients calculated for adsorption of BR 46.

Isotherm	**Parameters**	**Value**
Langmuir	Q_m (mg.g^{-1})	58.61
	K_a (L mg^{-1})	9.57
	R^2	0.999
Freundlich	1/n	0.362
	K_F (L mg^{-1})	4.12
	R^2	0.925
Temkin	B_1	5.85
	K_T(L mg^{-1})	2618.66
	R^2	0.884
Dubinin-radushkevich	Q_s (mg g^{-1})	50.94
	B × 10^{-9}	6.0
	E	4751.94
	R^2	0.947

Table 5. Comparison of adsorption performance of Ce-TiO_2-NPs-AC for ultrasound-assisted adsorption of BR 46 with other adsorbents.

Adsorbent	**Adsorption capacity Q_m (mg g^{-1})**	**pH**	**Time (min)**	**Ref.**
NiO-NPs-modified diatomite	72.46	8	60	[40]
Princess tree leaf	43.10	8	70	[41]
Pine tree leaves	71.94	6	75	[42]
Boron industry waste	74.73	9	60	[43]
Thin phosphate	28.57	8	<90	[44]
Raw phosphate	14.70	8	<90	[44]

Coarse phosphate	16.62	8	<90	[44]
Natural sugarcane stalks powder	20.96	7.2	60	[45]
Moroccan clay	54.00	–	20	[46]
Activated carbon	26.41	5	4	This work
TiO_2- NPs-AC	49.05	5	4	This work
Ce-TiO_2-NPs-AC	58.61	5	4	This work

3.7. Reusability of Ce-TiO_2-NPs-AC

The regeneration of Ce-TiO_2-NPs-AC is checked for several consecutive applications in adsorption experiments, following washing with ethanol. The experimental results—according to *t*-test—confirm good reusability up to four consecutive cycles, as shown in Fig. 5. The good reusability of Ce-TiO_2-NPs-AC is due to the nanometer-sized structure with a high surface area, which, in combination with its lower cost, lead to reduction of the overall cost of the adsorption process.

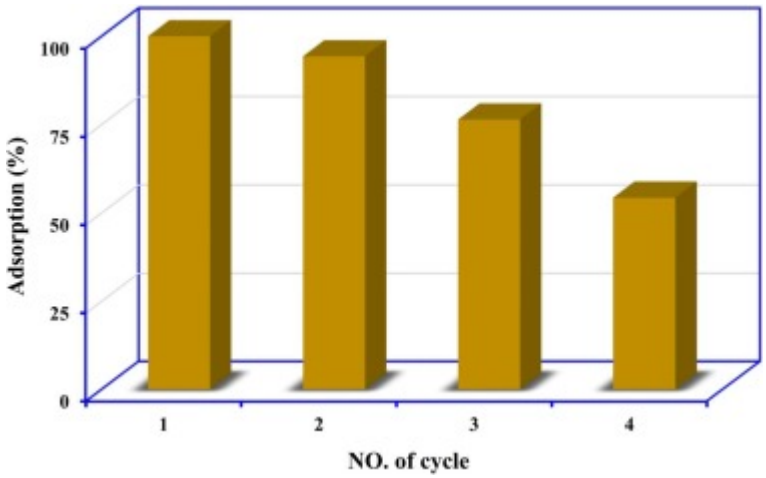

Fig. 5. Reusability of Ce-TiO_2-NPs-AC for BR 46 adsorption.

4. Conclusion

The primary goal of this work is the ultrasound-assisted synthesis of Ce-TiO_2-NPs-AC and verification of its applicability for BR 46 removal from aqueous solution. The effect of different parameters (e.g. BR 46 content, pH of solution, adsorbent mass, and ultrasound time) was studied using CCD. The 3D surface plots showed that BR 46 adsorption had a maximum value with a higher content of adsorbent; nonetheless, the same conditions and higher concentration of BR 46 led to decrease in removal percentage. The very rapid adsorption rate at lower time was because of the high surface area as well as the vacant adsorbent sites, which allow for increasing contact between dye and adsorbent after exposure to ultrasound power. The Langmuir, in comparison to other models, has more ability to fit and represent experimental data with monolayer adsorption capacity of 58.61 mg g^{-1}. The BR 46 adsorption onto Ce-TiO_2-NPs-AC efficiency was predicted by pseudo second-order model. The adsorbent presented here is a constant, an effective, an inexpensive, a green, and an eco-friendly material. The equilibrium was achieved in a much shorter time, and a significant amount of BR 46 was adsorbed on Ce-TiO_2-NPs-AC compared to other adsorbents reported in the literature.

Acknowledgements

The authors express their appreciation to the Graduate School and Research Council of the University of Yasouj for financial support of this work.

References

[1] K.B. Tan, M. Vakili, B.A. Horri, P.E. Poh, A.Z. Abdullah, B. Salamatinia. **Adsorption of dyes by nanomaterials: recent developments and adsorption mechanisms.** *Sep. Purif. Technol*., 150 (2015), pp. 229-242

[2] Z. Aksu. **Application of biosorption for the removal of organic pollutants: a review.** *Process Biochem*., 40 (2005), pp. 997-1026

[3] E.A. Dil, M. Ghaedi, A. Ghaedi, A. Asfaram, A. Goudarzi, S. Hajati, M. Soylak, S. Agarwal, V.K. Gupta. **Modeling of quaternary dyes adsorption onto ZnO–NR–AC artificial neural network: analysis by derivative spectrophotometry.** *J. Ind. Eng. Chem*., 34 (2016), pp. 186-197

[4] H. Xie, Q. Zhao, Z. Zhou, Y. Wu, H. Wang, H. Xu. **Efficient removal of Cd (II) and Cu (II) from aqueous solution by magnesium chloride-modified Lentinula edodes.** *RSC Adv*., 5 (2015), pp. 33478-33488

[5] A. Asfaram, M. Ghaedi, S. Agarwal, I. Tyagi, V. Gupta. **Removal of basic dye Auramine-O by ZnS: Cu nanoparticles loaded on activated carbon: optimization of parameters using response surface methodology with central composite design.** *RSC Adv*., 5 (2015), pp. 18438-18450

[6] A. Asfaram, M. Ghaedi, F. Yousefi, M. Dastkhoon. **Experimental design and modeling of ultrasound assisted simultaneous adsorption of cationic dyes onto ZnS: Mn-NPs-AC from binary mixture.** *Ultrason. Sonochem*., 33 (2016), pp. 77-89

[7] S. Rangabhashiyam, N. Anu, M.G. Nandagopal, N. Selvaraju. **Relevance of isotherm models in biosorption of pollutants by agricultural byproducts.** *J. Environ. Chem. Eng*., 2 (2014), pp. 398-414

[8] T.A. Saleh, A. Sarı, M. Tuzen. **Effective adsorption of antimony (III) from aqueous solutions by polyamide-graphene composite as a novel adsorbent.** *Chem. Eng. J.,* 307 (2017), pp. 230-238

[9] E. Altıntıg, H. Altundag, M. Tuzen, A. Sarı. **Effective removal of methylene blue from aqueous solutions using magnetic loaded activated carbon as novel adsorbent.** *Chem. Eng. Res. Design*, 122 (2017), pp. 151-163

[10] M. Khajeh, M. Kaykhaii, A. Sharafi. **Application of PSO-artificial neural network and response surface methodology for removal of methylene blue using silver nanoparticles from water samples.** *J. Ind. Eng. Chem*., 19 (2013), pp. 1624-1630

[11] E. Alipanahpour Dil, M. Ghaedi, A. Asfaram, F. Mehrabi, F. Sadeghfar. **Efficient adsorption of Azure B onto CNTs/Zn:ZnO@Ni_2P-NCs from aqueous solution in the presence of ultrasound wave based on multivariate optimization.** *J. Ind. Eng. Chem*., 74 (2019), pp. 55-62

[12] F. Mehrabi, E.A. Dil. **Investigate the ultrasound energy assisted adsorption mechanism of nickel (II) ions onto modified magnetic cobalt ferrite nanoparticles: multivariate optimization.** *Ultrason. Sonochem*., 37 (2017), pp. 37-46

[13] E.A. Dil, M. Ghaedi, A. Asfaram, A.A. Bazrafshan. **Ultrasound wave assisted adsorption of congo red using gold-magnetic nanocomposite loaded on activated carbon: optimization of process parameters.** *Ultrason. Sonochem*., 46 (2018), pp. 99-105

[14] T.A. Saleh, M. Tuzen, A. Sarı. **Magnetic activated carbon loaded with tungsten oxide nanoparticles for aluminum removal from waters.** *J. Environ. Chem. Eng*., 5 (2017), pp. 2853-2860

[15] A. Asfaram, M. Ghaedi, S. Hajati, A. Goudarzi. **Synthesis of magnetic γ-Fe_2O_3-based nanomaterial for ultrasonic assisted dyes adsorption: modeling and optimization.** *Ultrason. Sonochem*., 32 (2016), pp. 418-431

[16] F. Mehrabi, A. Vafaei, M. Ghaedi, A.M. Ghaedi, E.A. Dil, A. Asfaram. **Ultrasound assisted extraction of Maxilon Red GRL dye from water samples using cobalt ferrite nanoparticles loaded on activated carbon as sorbent: optimization and modeling.** *Ultrason. Sonochem*., 38 (2017), pp. 672-680

[17] D.O. Aksoy, E. Sagol. **Application of central composite design method to coal flotation: modelling, optimization and verification.** *Fuel*, 183 (2016), pp. 609-616

[18] A. Witek-Krowiak, K. Chojnacka, D. Podstawczyk, A. Dawiec, K. Pokomeda. **Application of response surface methodology and artificial neural network methods in modelling and optimization of biosorption process.** *Bioresour. Technol*., 160 (2014), pp. 150-160

[19] E.A. Dil, M. Ghaedi, A. Ghaedi, A. Asfaram, M. Jamshidi, M.K. Purkait. **Application of artificial neural network and response surface methodology for the removal of crystal violet by zinc oxide nanorods loaded on activate carbon: kinetics and equilibrium study.** *J. Taiwan Inst. Chem. Eng*., 59 (2016), pp. 210-220

[20] E.A. Dil, M. Ghaedi, A. Asfaram, F. Mehrabi. **Application of modificated magnetic nanomaterial for optimization of ultrasound-enhanced removal of Pb^{2+} ions from aqueous solution under experimental design: investigation of kinetic and isotherm.** *Ultrason. Sonochem*., 36 (2017), pp. 409-419

[21] E.A. Dil, M. Ghaedi, G.R. Ghezelbash, A. Asfaram, A.M. Ghaedi, F. Mehrabi. **Modeling and optimization of Hg^{2+} ion biosorption by live yeast Yarrowia lipolytica 70562 from aqueous solutions under artificial neural network-genetic algorithm and response surface methodology: kinetic and equilibrium study.** *RSC Adv*., 6 (2016), pp. 54149-54161

[22] E.A. Dil, M. Ghaedi, A. Asfaram, F. Mehrabi, A.A. Bazrafshan. **Optimization of process parameters for determination of trace Hazardous dyes from industrial wastewaters based on nanostructures materials under ultrasound energy.** *Ultrason. Sonochem*., 40 (2018), pp. 238-248

[23] S. Shirsath, D. Pinjari, P. Gogate, S. Sonawane, A. Pandit. **Ultrasound assisted synthesis of doped TiO_2 nano-particles: characterization and comparison of effectiveness for photocatalytic oxidation of dyestuff effluent.** *Ultrason. Sonochem*., 20 (2013), pp. 277-286

[24] E.A. Dil, M. Ghaedi, A. Asfaram .**The performance of nanorods material as adsorbent for removal of azo dyes and heavy metal ions: application of ultrasound wave, optimization and modeling.** *Ultrason. Sonochem*., 34 (2017), pp. 792-802

[25] E.A. Dil, M. Ghaedi, A. Asfaram. **Application of hydrophobic deep eutectic solvent as the carrier for ferrofluid: a novel strategy for pre-concentration and determination of mefenamic acid in human urine samples by high performance liquid chromatography under experimental design optimization.** *Talanta*, 202 (2019), pp. 526-530

[26] E. Alipanahpour Dil, A. Asfaram, F. Sadeghfar. **Magnetic dispersive micro-solid phase extraction with the $CuO/ZnO@Fe_3O_4$-CNTs nanocomposite sorbent for the rapid pre-concentration of chlorogenic acid in the medical extract of plants, food, and water samples.** *Analyst*, 144 (2019), pp. 2684-2695

[27] A. Rai, B. Mohanty, R. Bhargava. **Supercritical extraction of sunflower oil: a central composite design for extraction variables.** *Food Chem.,* 192 (2016), pp. 647-659

[28] E. Sharifpour, H.Z. Khafri, M. Ghaedi, A. Asfaram, R. Jannesar. **Isotherms and kinetic study of ultrasound-assisted adsorption of malachite green and Pb^{2+} ions from aqueous samples by copper sulfide nanorods loaded on activated carbon: experimental design optimization.** *Ultrason. Sonochem*., 40 (2018), pp. 373-382

[29] G. Crini, P.-M. Badot. **Application of chitosan, a natural aminopolysaccharide, for dye removal from aqueous solutions by adsorption processes using batch studies: a review of recent literature.** *Prog. Poly. Sci.,* 33 (2008), pp. 399-447

[30] Y. Cheng, T. Huang, X. Shi, G. Wen, Y. Sun. **Removal of ammonium ion from water by Na-rich birnessite: performance and mechanisms.** *J. Environ. Sci.,* 57 (2017), pp. 402-410

[31] Y. Ho, J. Ng, G. McKay. **Kinetics of pollutant sorption by biosorbents.** *Sep. Purif. Methods*, 29 (2000), pp. 189-232

[32] Y.-S. Ho. **Review of second-order models for adsorption systems.** *J. Hazard. Mater*., 136 (2006), pp. 681-689

[33] F.-C. Wu, R.-L. Tseng, R.-S. Juang. **Characteristics of Elovich equation used for the analysis of adsorption kinetics in dye-chitosan systems.** *Chem. Eng. J.,* 150 (2009), pp. 366-373

[34] W.J. Weber, J.C. Morris. **Kinetics of adsorption on carbon from solution.** *J. Sanit. Eng. Div*., 89 (1963), pp. 31-60

[35] I. Langmuir. **The adsorption of gases on plane surfaces of glass, mica and platinum.** *J. Am. Chem. Soc*., 40 (1918), pp. 1361-1403
[36] H. Freundlich. **Over the adsorption in solution.** *J. Phys. Chem*., 57 (1906), pp. 1100-1107
[37] A. Shamsizadeh, M. Ghaedi, A. Ansari, S. Azizian, M.K. Purkait. **Tin oxide nanoparticle loaded on activated carbon as new adsorbent for efficient removal of malachite green-oxalate: non-linear kinetics and isotherm study.** *J. Mol. Liq*., 195 (2014), pp. 212-218
[38] M. Temkin, V. Pyzhev. **Recent modifications to Langmuir isotherms.** *Acta Phys.-Chim. Sin*., 12 (1940), pp. 217-222
[39] M.M. Dubinin, L. Radushkevich. **Equation of the characteristic curve of activated charcoal.** *Chem. Zentr*, 1 (1947), p. 875
[40] R.K. Sheshdeh, M.R.K. Nikou, K. Badii, N.Y. Limaee, G. Golkarnarenji. **Equilibrium and kinetics studies for the adsorption of Basic Red 46 on nickel oxide nanoparticles-modified diatomite in aqueous solutions.** *J. Taiwan Inst. Chem. Eng*., 45 (2014), pp. 1792-1802
[41] F. Deniz, S.D. Saygideger. **Removal of a hazardous azo dye (Basic Red 46) from aqueous solution by princess tree leaf.** *Desalination*, 268 (2011), pp. 6-11
[42] F. Deniz, S. Karaman. **Removal of Basic Red 46 dye from aqueous solution by pine tree leaves.** *Chem. Eng. J*., 170 (2011), pp. 67-74
[43] A. Olgun, N. Atar. **Equilibrium and kinetic adsorption study of Basic Yellow 28 and Basic Red 46 by a boron industry waste.** *J. Hazard. Mater*., 161 (2009), pp. 148-156
[44] Z. Graba, S. Hamoudi, D. Bekka, N. Bezzi, R. Boukherroub. **Influence of adsorption parameters of basic red dye 46 by the rough and treated Algerian natural phosphates.** *J. Ind. Eng. Chem*., 25 (2015), pp. 229-238
[45] G.O. El-Sayed, T.Y. Mohammed, A.A.-A. Salama. **Batch Adsorption of maxilon red GRL from aqueous solution by natural sugarcane stalks powder.** *ISRN Environ. Chem*., 2013 (2013)
[46] A.B. Karim, B. Mounir, M. Hachkar, M. Bakasse, A. Yaacoubi. **Removal of Basic Red 46 dye from aqueous solution by adsorption onto Moroccan clay.** *J. Hazard. Mater*., 168 (2009), pp. 304-309